https://doi.org/10.1016/j.enbuild.2021.111688

Scaled outdoor experimental analysis of ventilation and interunit dispersion with wind and buoyancy effects in street canyons

Yuwei Dai[a,b], Cheuk Ming Mak[b]*, Jian Hang[c,d], Fuyao Zhang[a], Hong Ling[c,d]

[a]School of Environment and Architecture, University of Shanghai for Science and Technology, 516 Jungong Rd., Shanghai, China

[b]Department of Building Environment and Energy Engineering, The Hong Kong Polytechnic University, Hong Kong, China.

[c]School of Atmospheric Sciences, Guangdong Province Key Laboratory for Climate Change and Natural Disaster Studies, Sun Yat-sen University, Guangzhou, P.R. China 510275.

[d]Key Laboratory of Tropical Atmosphere-Ocean System (Sun Yat-sen University), Ministry of Education, Zhuhai (519000), China

*Corresponding author: Cheuk Ming Mak

Email: cheuk-ming.mak@polyu.edu.hk

Abstract

Driven by wind and buoyancy effects in the urban environment, ventilation performance and pollutant transmission are highly related to human health. In order to investigate characteristics of the single-sided natural ventilation and interunit dispersion problem, this study conducted scaled outdoor experiments in summer and winter periods in two-dimensional street canyons. Tracer gas method was adopted to predict the ventilation rate and simulate the pollutant dispersion. It was found the ventilation performance of windward and leeward rooms showed different trends with wind velocities. Archimedes number Ar was used to examine the interactions of the buoyancy and the wind forces. It revealed that the non-dimensional ventilation rates of all rooms were generally smaller than the results of buoyancy effect only. It indicates that interactions between the buoyancy and wind effects were destructive, which reduced the ventilation rates. The interunit dispersion characteristics with the wind effect were highly dependent on source locations. The results of the tracer gas concentrations of the reentered rooms were not showing simple increasing or decreasing trends. This study provides authentic and instant airflow and pollutant dispersion information in an urban environment. The dataset of this experiment can offer validations for further numerical simulations.

Keywords: scaled street canyon, ventilation, interunit dispersion, buoyancy effect, urban environment.

Nomenclature

ACH	air exchange
Ar	Archimedes number

A_w	window area (m^2)
C_D	discharge coefficient, 0.6
C_{in}	indoor CO_2 concentration (ppm)
C_{in,t_i}	tracer gas concentration at time t_i (ppm)
$C_{in,t_{i+1}}$	tracer gas concentration at time t_{i+1} (ppm)
C_{out}	CO_2 concentration in ambient fresh air (ppm)
C_s	source concentration (ppm)
g	gravitational acceleration (m^2/s)
H	building height, 1.2m
H_w	window height (m)
K_c	non-dimensional concentration
L	left side
Q	airflow rate of the room (m^3/s)
Q^*	non-dimensional ventilation rate
Q_B	flow rate caused by buoyancy effect (m^3/s)
${Q_B}^*$	non-dimensional ventilation rate of buoyancy effect
Q_s	emission rate of the tracer gas source (m^3/s)
R	right side
Re	Reynolds number
T_{inZ}	indoor air temperature on each floor (℃)
T_{outZ}	outdoor air temperature at the corresponding height (℃)
ΔT	temperature difference (K)
Δt	time interval (s)
U	wind velocity component (m/s)
$\overline{U}$	average incoming wind velocity (m/s)
U_{ref}	freestream velocity (m/s)
V	volume of the room (m^3)
V_i	volume of the reentered room (m^3)
W	width of the street canyon (m)
β	thermal expansion coefficient $(1/K)$
ϑ	turbulent viscosity (m^2/s)

1. Introduction

1.1 Background

Public health has been threatened by the outbreak of infectious diseases frequently in recent years, such as the coronavirus disease (COVID-19) pandemic occurred at the end of 2019, which has caused millions of death globally [1]. There exist three major routes for spreading such infectious diseases, namely direct-contact transmission, large droplet-contact transmission, and airborne transmission. While the transmission via direct and large droplet contact occurs in a short distance, the airborne transmission via aerosols can spread over an essentially longer distance and time [2, 3]. Available epidemiological and experimental evidence has implicated the airborne transmission is responsible for the spread of various infectious diseases [4-6] and would lead to a mass outbreak of community infection [7, 8]. In terms of airborne transmission, the indoor spread is considered as the dominant transmission pattern, however, the coupled indoor and outdoor transmission, called interunit dispersion, cannot be underestimated. The interunit dispersion is defined as the pathogen spread across the apartment units in a building. This transmission pattern has been revealed after the epidemiological examination of the SARS outbreak in the Amoy Gardens estate in Hong Kong in 2003 [9], which is highly risky because of the relatively short dispersion distances and transportation time, especially in densely populated areas.

1.2 State of the arts

The interunit dispersion problem, as a potential hazard, has gained popularity in recent years. Natural ventilation is a predominant driving force for interunit dispersion. Three methods, on-site measurement, wind tunnel experiment, and Computational Fluid Dynamics (CFD) simulation, have been mainly adopted to investigate such coupled indoor and outdoor airflow and pollutant dispersion phenomena. Related studies are summarized in Table 1. Niu and Tung [10] conducted on-site measurements in a 3-story building to investigate the vertical interunit dispersion mechanism. They proposed a possible pollutant transmission route in a residential building and found that the percentage of the exhaust air from a lower unit to the immediate upper unit can reach 7%. Gough et al. [11] took full-scaled field measurements to investigate the characteristics of both single-sided and cross ventilation in an idealized building. Later, Wu et al. [12, 13] studied the internal spread route between horizontal adjacent rooms induced by air infiltrations with another on-site measurement in a 16-story residential building and then compared the contributions of the thermal buoyancy force and the wind force. They found that the wind effect played the dominant role in the interunit transmission [13].

Wind tunnel experiments [14-16] were also carried out to investigate the interunit dispersion problem. These studies mainly focused on the wind-dominated effects on multistory residential buildings with various wind directions and source locations. They concluded that, with the wind effect, the pollutant released from a single room may spread multi-directionally in the same building.

CFD simulation was more commonly used than on-site measurement and wind tunnel experiments because of its efficiency and cost-effectiveness. Different influential parameters were considered, such as the effects of buoyancy-dominated forces [17-21], balconies [22-24], window configurations[25, 26], surrounding interfering buildings [27, 28], and heated walls [29]. Former studies adopted several turbulence models, an advanced RANS model with a steady process [22, 24-28] and an LES model with a transient process [23, 30], to conduct the airflow and dispersion simulations. Based on the hypothetic atmospheric boundary conditions, the results of the ventilation performance and pollutant dispersion in different CFD simulations varied drastically and relied on the arrangement of the building models.

Recently, an effective alternative, known as the scaled outdoor experiment, has been adopted. Dallman et al. [31] investigated the airflow field and thermal effects in a mock street canyon constructed by two rows of shipping containers. Yee and Biltoft [32] investigated the characteristics of pollutant dispersion through a 10 × 12 array of building-like obstacles. Chen et al. [33, 34] studied the thermal conditions in the urban environment by performing scaled outdoor measurements. These researches reveal that the scaled outdoor experiment is a good option to perform parametric experimental studies of the wind and thermal problems. However, these studies mainly investigated purely outdoor problems. The scaled experiment can also be used to study the ventilation and pollutant transmission problems in the coupled outdoor and indoor conditions.

In order to investigate the ventilation and interunit dispersion problem, our previous study conducted the scaled outdoor experiment in idealized two-dimensional (2D) street canyons on the Scaled Outdoor Model Urban Climate and Health (SOMUCH) field at Sun Yat-sen University [35]. The 2D street canyon is defined as an infinitely long street canyon with buildings on both sides, while the approaching wind is perpendicular to the street axis [34]. Due to the simplicity and fundamentality of the geometry, the 2D street canyon has been widely adopted to investigate the flow and dispersion mechanism in the urban area [36]. This experiment lasted from June 8 to 10, 2019 in Guangzhou, which was on typical summer days. The tracer gas concentration was monitored in each room of the street canyons to simulate the pollutant dispersion routes, as well as the wind velocity and thermal conditions inside and outside the scaled models. The results showed that the tracer gas was mainly transported in the vortex direction inside the street canyon, and the maximum reentry ratio can be up to 17.7% under a certain wind condition. More recently, Yang et al. [37] used the tracer gas decay method to measure the ventilation rates of the rooms in street canyons at this scaled outdoor field. They mainly investigated the natural ventilation of different street canyon aspect ratios. In addition, Liu et al. [38] conducted a scaled multi-room chamber experiment to study the airflow characteristics and pollutant dispersion process.

Based on the real-time weather conditions and tracer gas concentration in the scaled outdoor experiment, it has been found the characteristics of tracer gas transmission are highly associated with the wind conditions [35]. With the continuously fluctuating incoming wind conditions, the results of the concentration dispersion are complicated. Therefore, it is necessary to investigate the detailed correlation between airborne transmission and wind conditions. Furthermore, the former outdoor experiment was conducted during the summer season, which represented one type of indoor and outdoor thermal conditions. The buoyancy effect caused by the temperature differences may also alter the tracer gas conditions in each room, but this driving force was not analyzed thoroughly in our previous work. Therefore, identifying the interactions of the wind effect and buoyancy effect to the ventilation and tracer gas dispersion is another important issue.

Table 1 A summary of the investigation in ventilation and pollutant dispersion with different methods.

Methodology	Features of investigation	References
On-site measurement	Vertical interunit dispersion	Niu and Tung [10]
	Single-sided and cross ventilation	Gough et al. [11]
	Internal pollutant spread route	Wu et al. [12,13]
Wind tunnel experiment	Pollutant dispersion with effect of wind directions	Wang et al. [14]
	Pollutant transmission with effect of source location	Mu et al. [15]
	Indoor pollutant dispersion and cross-contamination	Liu et al. [16]
CFD simulation	Effects of buoyancy-dominated forces	Li and Mak [17] Liu et al. [18] Gao et al. [19,20] Yang et al. [21]
	Effects of balconies	Ai et al. [22-24]
	Effects of window configurations	Wang et al. [25,26]
	Effects of surrounding interfering buildings	Cui et al. [27] Dai et al. [28]
	Effects of heated walls	Mu et al. [29]
Scaled outdoor experiment	Airflow field and thermal effects	Dallman et al. [31]
	Characteristics of pollutant dispersion	Yee and Biltoft [32]
	Thermal conditions with different aspect ratios	Chen et al. [33, 34]
	Ventilation with different aspect ratios	Yang et al. [37]
	Airflow characteristics and pollutant dispersion	Liu et al. [38]

1.3 Study aim and structure

This work aims to investigate the combined wind and buoyancy effect on the single-sided ventilation and interunit dispersion problems. For this objective, another outdoor experiment was conducted in the winter season (December 17 to 19, 2019) to change the thermal conditions. The main novelties of the present work can be summarized as (a) the scaled outdoor experiment data of wind and thermal conditions were investigated simultaneously with the tracer gas concentrations; (b) the datasets were compared with the summer experiment to study the interactions of wind and thermal effects; (c) the characteristics of the two driving forces on the ventilation and dispersion were analyzed in the scaled street canyons. This study intended to provide a complementary method between the on-site measurements and numerical simulations of ventilation problems in street canyons. This work provides authentic airflow and pollutant dispersion information under an urban environment. In addition, the dataset of this experiment can offer validation for further numerical simulations.

The rest of this paper is organized as follows: Section 2 introduces the experiment setting and analysis methodology. Detailed results and discussions are presented in

Section 3. Section 4 discusses the limitations of the current study and future works, and section 5 summarizes and concludes this study.

2. Methodology

The scaled outdoor experiments have been adopted recently as a useful alternative. The main advantages of this method are: (a) this method can reduce the geometry uncertainties of the on-site measurements; (b) it can mitigate some ambiguities of the wind tunnel and numerical simulations. In the present work, scaled outdoor experiments were conducted at SOMUCH experimental field, which is located on the southern side of Guangzhou, China ($23°01'N$, $113°24'E$). According to Köppen-Geiger climates Classification [39], the climate in Guangzhou can be classified as Cfa, which is a humid subtropical climate [40, 41]. The climate is mild, generally warm and temperate. The average annual temperature is 22.4 °C in Guangzhou.

2.1 Experiment setup

2.1.1 Description of the SOMUCH experimental field

In order to simulate a generalized street canyon in the urban environment, this experiment field is built on a $57\ m \times 57.5\ m$ concrete foundation and contains more than 2000 concrete models. The concrete model is customized as a hollow cuboid with length × width × height $= 0.5\ m \times 0.5\ m \times 1.2\ m$. The concrete models are painted dark gray as ordinary urban buildings and have a wall thickness of $1.5\ cm$. The whole north/south street canyon field is width × length $= 44.4\ m \times 12\ m$, the street canyon deviates by around $30°$ from the northern direction, as shown in Fig. 1 (a) and (b). The street canyon consists of 34 arrays of cuboids with 4 aspect ratios (H/W) of 1, 2, 3, and 6, accordingly. Each aspect ratio contains six street canyons and each row has 24 building models. This study chose a $1:1$ street canyon as the target area to conduct the experiment. The measurements consisted of two sections, the first section lasted from June 8 to 10, 2019 in the typical summer season, the second section lasted from December 17 to 19, 2019 in the typical winter season; on each day, the measurements lasted around from 9 am to 10 pm.

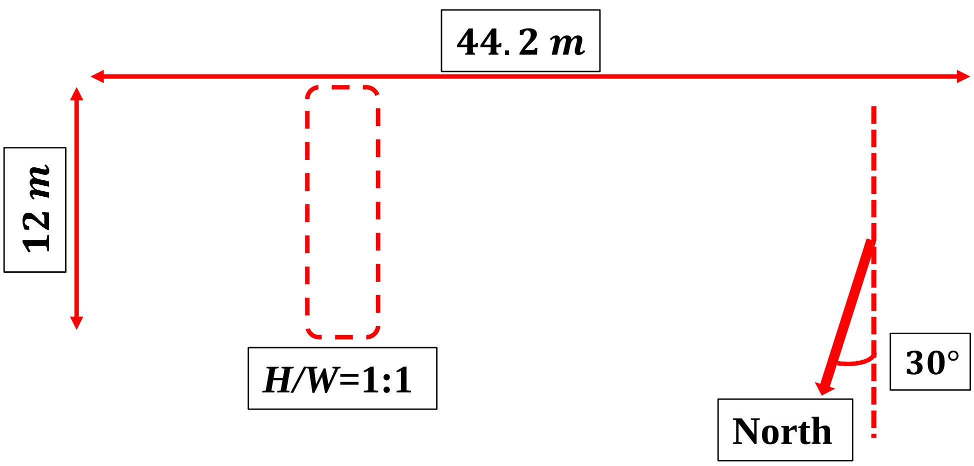

(a)

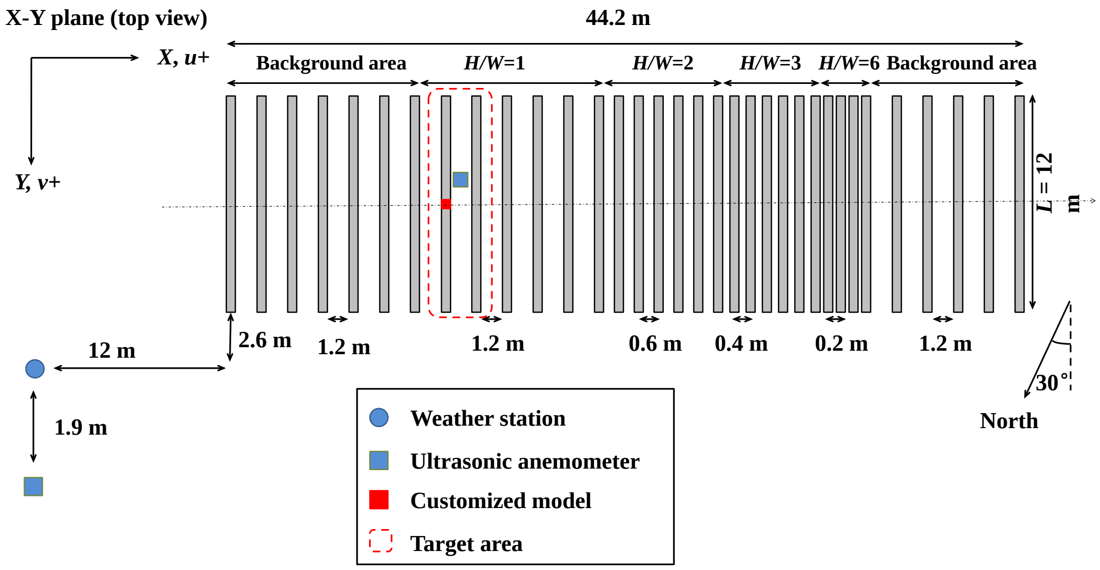

(b)

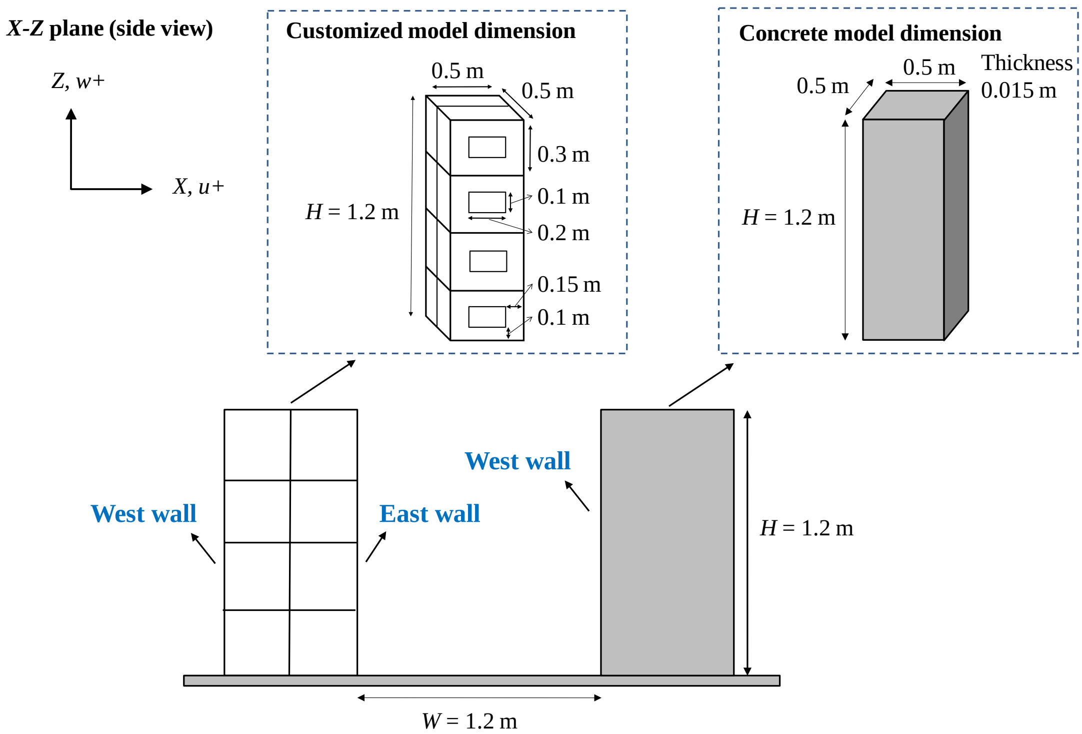

(c)

Fig. 1 (a) Overview of the experiment field; (b) Schematic view of the experiment field on X–Y plane and instrument positions; (c) Dimensions of the customized and concrete models on X–Z plane of the target street canyon.

2.1.2 Description of the building model

In order to investigate the coupled indoor and outdoor pollutant dispersion, an acrylic model ($5mm$ of thickness) was customized with a total of eight rooms, which had the same dimension as the concrete models. This customized model had four floors and each floor had two rooms with opposite window openings. The height and width of each opening were $0.1\ m$ and $0.2\ m$, respectively, as shown in Fig. 1 (c). This model can represent a typical single-sided ventilation building. The opening-to-wall ratio for the current model was 13.3% which was considered large. The acrylic model was covered with tinfoil to avoid the greenhouse gas effect and placed in the middle of the street canyon with a $1:1$ aspect ratio, as shown in Fig. 1 (b).

2.2 Measured parameters and instrumentation

In this experiment, carbon dioxide (CO_2) was used as the tracer gas, which had the availability of multiple measuring points (eight points at the same time) and a short response time ($1s$). Sonic anemometers (Gill WindMaster), thermocouples (Omega, TT-K-36-SLE, $\Phi\ 0.127mm$), weather stations (RainWise PortLog) and CO_2 sensors (HR International Co.) were used to measure the three wind velocity components (u, v, w) and turbulence, air/wall temperatures, background atmospheric condition, and CO_2 concentrations, respectively. The detailed specifications of the instrumentations used in the experiment are given in Table 2.

A weather station (RainWise PortLog) was used to measure the background air temperature, wind velocity, and wind direction, the position at the field was shown in Fig. 1(b). The time interval was set as 1min. The sensor of the weather station was placed at a height of 2.4 m (2 times the model height) [33, 42].

Table 2 Summary of parameters measured and equipment used.

Parameters	Equipment	Manufacturing company	Accuracies	Sampling rate
Wind velocity/ direction	3D ultrasonic anemometer	Gill Instruments Limited.	1.5% in a range of $0-50m/s$, $2°$ in range of 0~359.9°	20Hz
Indoor/outdoor air temperature and wall temperature	K type fine-wire thermocouple ($\Phi\ 0.127mm$)	Agilent Technologies Inc. (Data logger)	1.1℃ or 0.4% in a range of $-200-260$℃, refer to the greater one	1s
CO_2 concentration	CO_2 sensor	HR International Co.	$\pm 40ppm$ in a range of $400-10000ppm$	1s
Background air temperature,	Automatic weather station	RainWise Inc.	± 0.25℃ in range of $-54-74$℃, $\pm 2\%$ in	1min

wind speed and direction			range of $0-67m/s$, $3°$ in range of 0~360°	

As shown in Fig. 2(c), two wind masts, each equipped with five ultrasonic anemometers, were planted on the field. One wind mast with a $10\ m$ height was used to measure the far-field incoming flow velocities; another was used to measure the wind velocities in the middle of the street canyon. Noted that, the arrangements of ultrasonic anemometer of the two experiments (summer and winter) were different. In the summer experiment, the five ultrasonic anemometers of $10m$ wind mast were placed at 0.6, 1.2, 2.4, 5, and $10m$, as shown in Fig. 2(a). While the anemometers of wind mast in the street canyon were placed at 0.15, 0.45, 0.75, 1.05, and $2.4m$, as shown in Fig. 2(b). The detailed information on the wind conditions of the summer period can be found in our previous paper [35]. In the winter experiment, because of the limited instruments, the number of ultrasonic anemometers of $10\ m$ wind mast reduced to three, which were placed at 2.4, 5, and $10m$, as shown in Fig. 2(c), and anemometers of wind mast in the street canyon were also placed at three positions of 0.15, 0.45, and $0.75m$, as shown in Fig. 2(d).

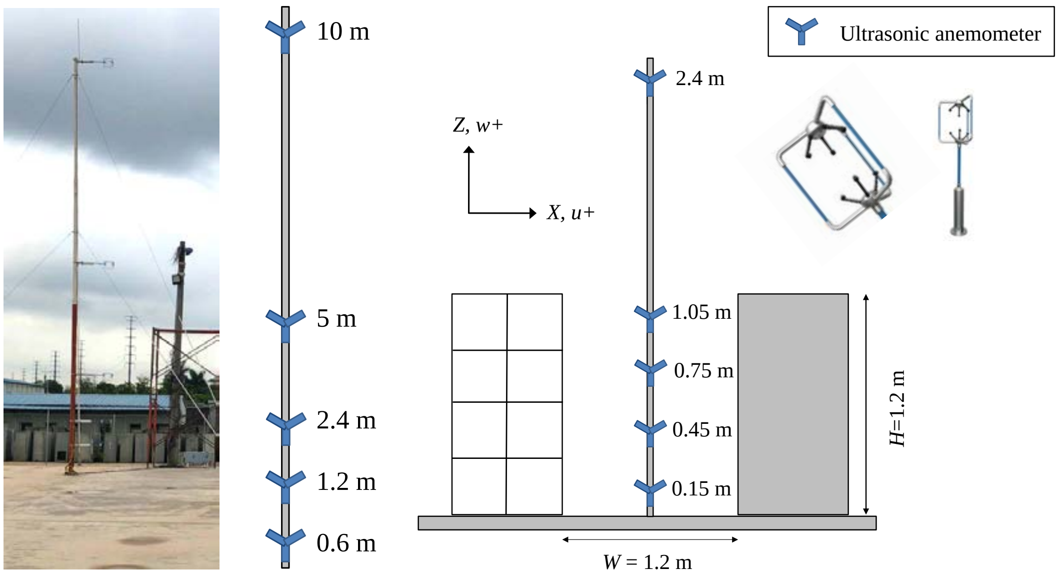

(a) (b)

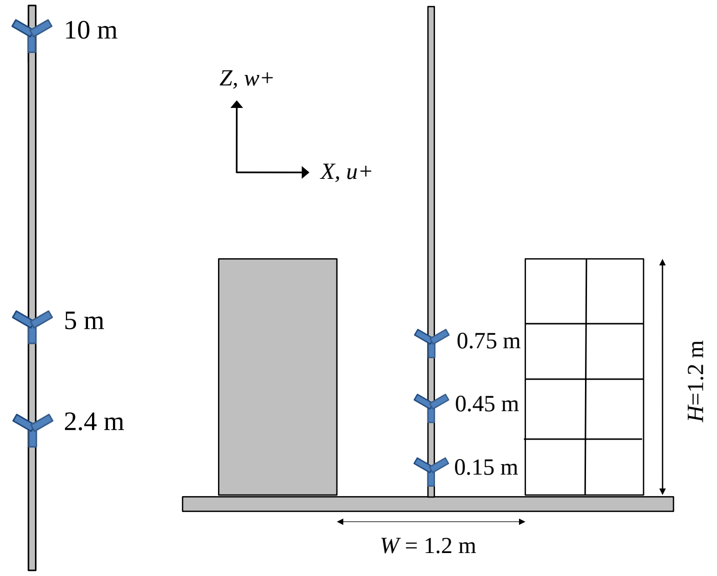

(c) (d)

Fig. 2 Schematic view of the wind masts and ultrasonic anemometer positions: (a) 10-m mast in summer experiment; (b) 2.4-m mast in summer experiment; (c) 10-m mast in winter experiment; (d) 2.4-m mast in winter experiment.

Eight CO_2 sensors were placed near the opening of each room to measure the indoor concentration with the inlet side of the CO_2 sensor faced the opening, as shown in Fig. 3(a). CO_2, the tracer gas, was transported into the source room via a long tube with a diameter of $8mm$ from a compressed gas cylinder. A customized plastic ball was installed at the end of the tube near the center of the source room to diminish the injection velocity. The diameter of the plastic ball was $30mm$. Six uniformly arranged holes with diameters of $5mm$ were drilled in the plastic ball for the multi-directional release of the tracer gas, as shown in Fig. 3(c).

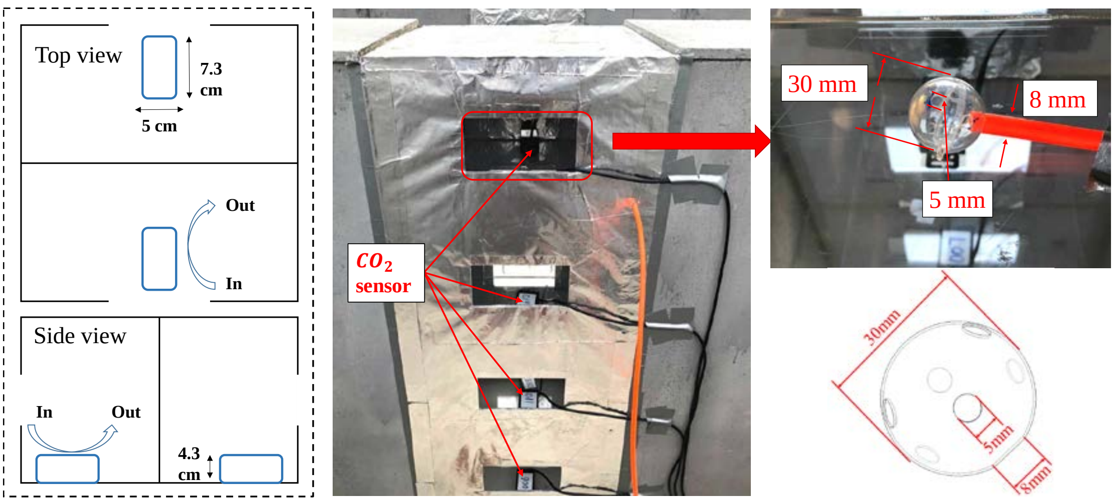

(a) (b) (c)

Fig. 3 Setup for the tracer gas release and concentration measurement: (a) Schematic view of positions of the CO_2 sensors in each room, In: inlet of the CO_2 sensor, Out: outlet of the CO_2 sensor; (b): Overview of the measurement setup; (c): Schematic view of the customized plastic ball.

The scaled model was made of acrylic with $5mm$ thickness, which makes the net volume of the room slightly smaller than the calculated result. Also, the CO_2 sensors (length×width×height= $7.3cm \times 5cm \times 4.3cm$), gas tube (diameter of $8mm$) and plastic ball (diameter of $30mm$) were put in the room and accounted for certain volumes. Apart from the uncertainties of the equipment (see Table 2), the deviation of the estimated volume from the real volume was around 1%, which would propagate a 1.3% uncertainty to air exchange values of each test (calculated based on Equation 4).

Eight thermocouples (Omega, TT-K-36-SLE, $\Phi\ 0.127mm$) were placed in the middle of each room to measure the indoor air temperature, as shown in Fig. 4. Four thermocouples were placed in the middle of the street canyon to measure the outdoor air temperature at various heights ($z = 0.15,\ 0.45,\ 0.75,\ 1.05m$). Eight thermocouples were mounted on the vertical walls to measure the surface temperatures of the building model at the same heights. These temperature data were recorded by Agilent 34972A data loggers at intervals of $1s$ continuously.

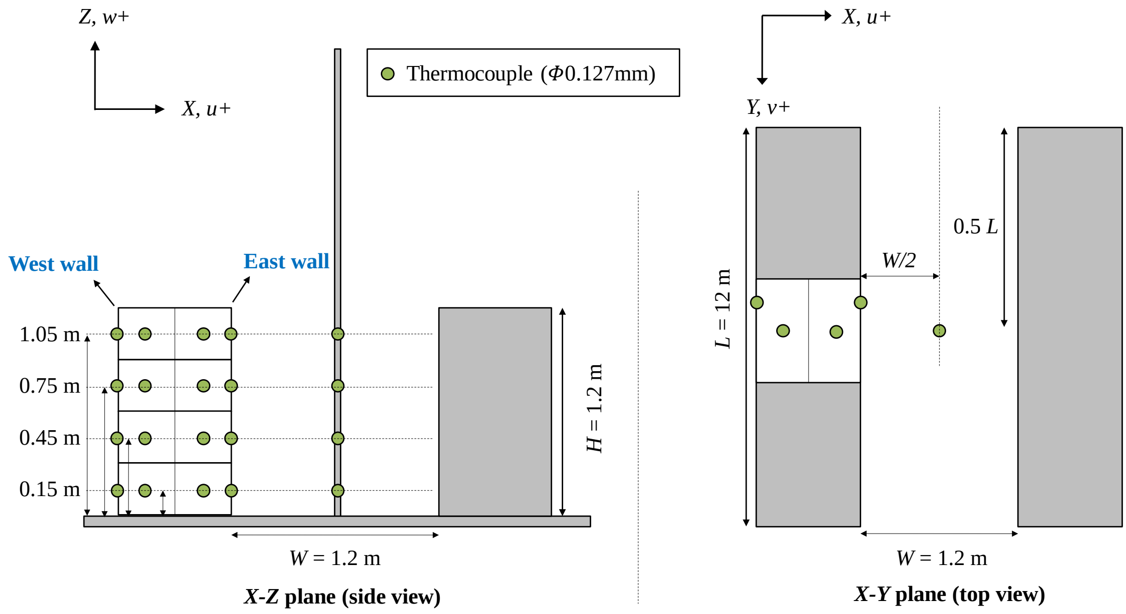

Fig. 4 Schematic view of the thermocouple positions in the target street canyon on X-Z plane and X-Y plane.

2.3 Experiment design

As shown in Fig. 5(a), R represents the right side, and L represents the left side, from the Northside view. Noted that, since the wind directions and velocities fluctuated during the experiment periods, the windward and leeward sides of the building model were hard to be determined simply by the room locations. Therefore, the results will be analyzed according to the wind direction of each test. The wind information will be elaborated in section 3.1. During the tests, each room was set as the source room multiple times. The concentration of the source gas was $10^5 ppm$. The sampling frequency was $1 Hz$ and the output results were averaged for $1 s$. In the summer experiment (June 8 to 10, 2019), the tracer gas was released continuously for around $30\ min$, and the flow rate was $1.5 L/min$. While in the winter experiment (December 17 to 19, 2019), the tracer gas was released for at least $20 min$, and the flow rate was $1.0 L/min$.

All instruments were sampled simultaneously for the wind velocity, wind direction, air/wall temperatures, and CO_2 concentrations in each room. After completing one test, the gas releasing tube was pulled out. The next test was not initiated until the CO_2 concentration in the former source room declined to the background level. A flow chart of the experiment process is summarized in Fig. 5(b). Each room as a source location was a single test, Table 3 lists the information of all tests during the two experiment periods (June 8 to 10, 2019 and December 17 to 19, 2019).

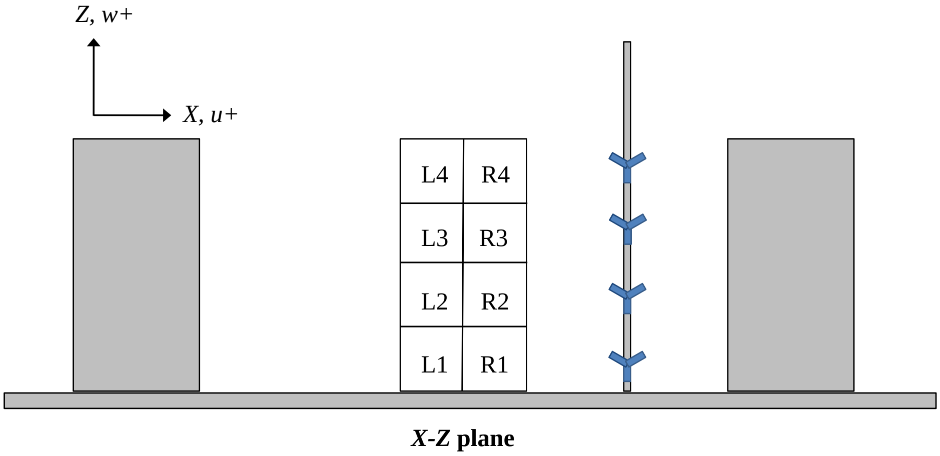

(a)

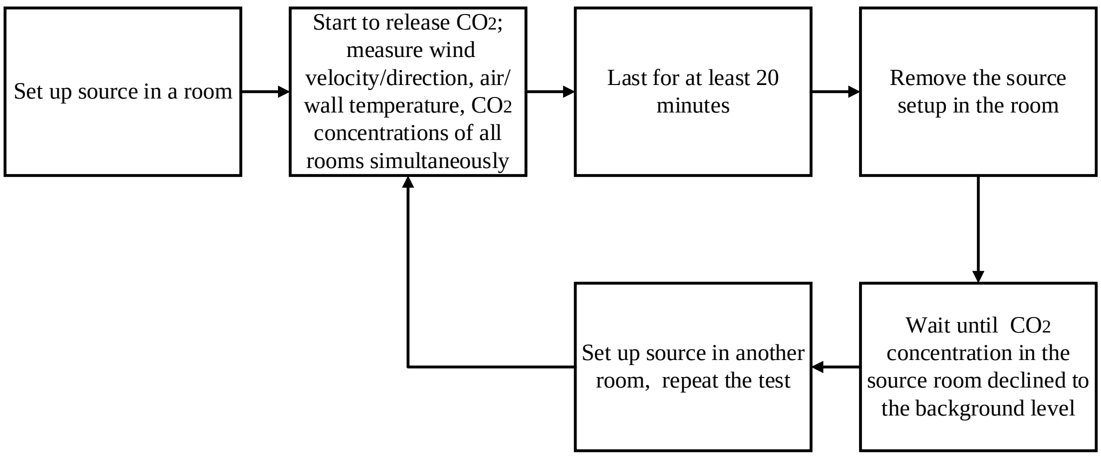

(b)

Fig. 5 (a) Side view of eight rooms in the target street canyon; (b) Flow chart of the experiment process.

Table 3 Summary of the tests from two experiment periods (June 8 to 10, 2019 and December 17 to 19, 2019).

Source Room	Period	Date	Time	Number	Source Room	Period	Date	Time	Number
L1	Summer	8-Jun	09:46-10:16	L1-a	R1	Summer	8-Jun	18:57-19:28	R1-a
		9-Jun	14:16-14:46	L1-b			9-Jun	10:40-11:10	R1-b
		9-Jun	19:06-19:26	L1-c			10-Jun	12:19-12:49	R1-c
	Winter	17-Dec	10:47-11:07	L1-d		Winter	17-Dec	15:54-16:14	R1-d
		18-Dec	10:07-10:27	L1-e			18-Dec	15:28-15:48	R1-e
		19-Dec	15:37-15:58	L1-f			19-Dec	10:18-10:38	R1-f
L2	Summer	8-Jun	10:32-11:02	L2-a	R2	Summer	8-Jun	18:10-18:40	R2-a
		8-Jun	21:19-21:49	L2-b			9-Jun	11:32-12:02	R2-b
		9-Jun	15:11-15:41	L2-c			10-Jun	11:35-12:05	R2-c
	Winter	17-Dec	11:33-11:53	L2-d		Winter	17-Dec	14:47-15:07	R2-d
		17-Dec	18:32-18:52	L2-e			17-Dec	16:38-16:58	R2-e
		18-Dec	10:47-11:07	L2-f			18-Dec	14:46-15:06	R2-f
		18-Dec	19:01-19:23	L2-g			18-Dec	16:13-16:31	R2-g
		19-Dec	15:00-15:21	L2-h			18-Dec	16:52-17:13	R2-h
		19-Dec	16:16-16:36	L2-i			18-Dec	20:50-21:13	R2-i
							19-Dec	10:54-11:14	R2-j
L3	Summer	8-Jun	11:23-11:53	L3-a	R3	Summer	8-Jun	15:53-16:23	R3-a
		8-Jun	20:32-20:54	L3-b			9-Jun	12:27-12:57	R3-b
		9-Jun	16:13-16:43	L3-c			10-Jun	10:51-11:21	R3-c

	Winter	17-Dec	12:13-12:34	L3-d		Winter	17-Dec	14:10-14:30	R3-d
		17-Dec	17:52-18:12	L3-e			17-Dec	17:16-17:36	R3-e
		18-Dec	11:37-11:57	L3-f			18-Dec	13:58-14:18	R3-f
		18-Dec	18:15-18:35	L3-g			18-Dec	17:36-17:56	R3-g
		19-Dec	13:03-13:23	L3-h			18-Dec	21:28-21:48	R3-h
		19-Dec	16:50-17:12	L3-i			19-Dec	11:23-11:43	R3-i
L4	Summer	8-Jun	12:12-12:42	L4-a	R4	Summer	8-Jun	17:18-17:48	R4-a
		8-Jun	19:49-20:09	L4-b			9-Jun	13:19-13:49	R4-b
		9-Jun	17:09-17:39	L4-c			10-Jun	09:45-10:15	R4-c
	Winter	17-Dec	12:59-13:19	L4-d		Winter	17-Dec	13:40-14:00	R4-d
		18-Dec	12:18-12:47	L4-e			18-Dec	13:16-13:38	R4-e
		19-Dec	12:28-12:48	L4-f			19-Dec	11:54-12:17	R4-f

2.4 Similarity criteria

In order to obtain a similar airflow field in contrast to the real world, Reynolds number (Re) can be used as the similarity criterion, which is defined as

$$Re = \frac{U_{ref} H}{\nu} \quad (1)$$

where U_{ref} is the freestream velocity (m/s, velocities at 2.4m in this experiment), H is the street canyon height (m) and ν is the kinematic viscosity (m^2/s).

During the experimental period, the average freestream velocities of all tests are summarized in section 3.1. Except for test L3-e (17-Dec, 17:52-18:12, the average wind velocity was nearly zero), the minimum freestream velocity of other tests was $0.27 m/s$. The Reynolds number was 21441 as $U_{ref} = 0.27 m/s$, which can be considered sufficiently large to meet the Reynolds number independence requirement (i.e. $Re \gg 11000$) [43].

2.5 Data analysis method

This study adopted the tracer gas method to predict the air exchange rate and simulate the pollutant dispersion in buildings. Assuming a steady flow and well-mixed tracer gas of the source room, the calculation of the ventilation rate based on the principle of mass conservation can be achieved by the following equation:

$$V\frac{dC_{in}}{dt} = Q(C_{out} - C_{in}) + C_s \cdot Q_s \tag{2}$$

where C_{in} is the indoor CO_2 concentration (ppm), C_{out} is the CO_2 concentration in ambient fresh air (ppm), V is the volume of the room (m^3), Q is the airflow rate of the room (m^3/s), C_s is the tracer gas concentration at the source (ppm) and Q_s is the emission rate of the tracer gas source (m^3/s). The ventilation rate can be converted to air exchange (ACH), based on Equation (1), as

$$ACH = \frac{Q}{V} = \frac{\frac{dC_{in}}{dt} - \frac{C_s \cdot Q_s}{V}}{C_{out} - C_{in}} \tag{3}$$

During a period of $\Delta t = t_{i+1} - t_i$ (h), the ventilation rate of a room can be expressed as

$$ACH = \frac{C_s \cdot Q_s \cdot \Delta t - (C_{in,t_{i+1}} - C_{in,t_i})V}{(C_{in,t_i} - C_{out})\Delta t \cdot V} \tag{4}$$

where $C_{in,t_i}$and $C_{in,t_{i+1}}$ represent the tracer gas concentration (ppm) of the room at times t_i and t_{i+1}, respectively.

The average concentration of the reentered rooms is used as an indicator to assess tracer gas transportation between the source and other rooms, which is presented in a non-dimensional form as

$$K_c = \frac{C_{i,t_i} - C_{out}}{C_s} \cdot \frac{V_i}{Q_s \cdot \Delta t} \tag{5}$$

where C_{i,t_i} is the measured concentration (ppm) of the tracer gas in the reentered room at time t_i,Δt is the time interval (s), and V_i is the volume of the reentered room (m^3), respectively.

3. Results and discussions

3.1 Monitored wind conditions during two test periods

The wind rose maps and velocity frequencies during the two experiment periods on June 8 to 10 and December 17 to 19, 2019 are shown in Fig. 6, which were measured by the Rainwise weather station. The wind directions in this experiment field changed frequently, but the wind directions between $225–270°$ and $45–90°$ were dominant during the summer and winter experiment periods, respectively. It implies that the prevailing wind directions of the two periods were almost opposite and approximately perpendicular to the street canyon. The averaged summer wind velocities were larger than winter, the wind velocities of summer period were mainly below $4m/s$ and winter period were mainly below $3m/s$. Fig. 7 shows the 60s-averaged wind velocity component U (normal to the street canyons) at the height $2.4m$ of each measuring day measured by the ultrasonic anemometers. It is clearly shown that the wind conditions of the urban environment highly fluctuated among different measurement days, which will affect the ventilation performance and pollutant dispersion drastically.

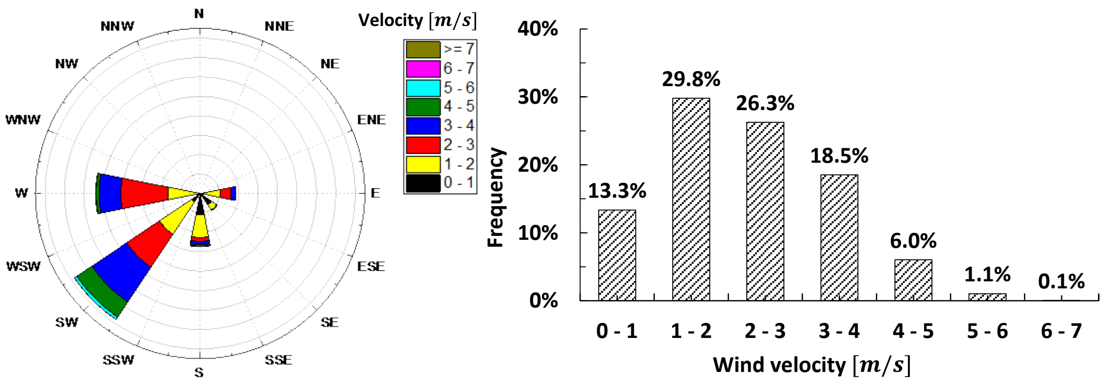

(a) June 8 to 10, 2019

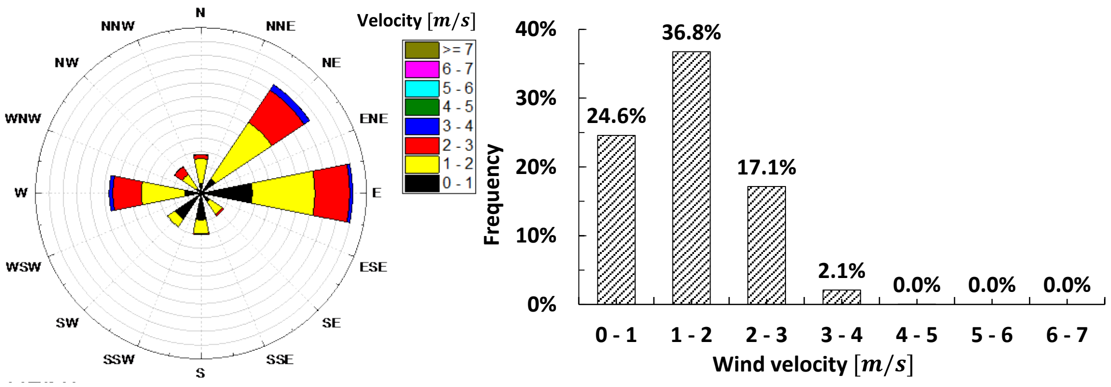

(b) December 17 to 19, 2019

Fig. 6 Wind rose maps and velocity frequencies during summer and winter measurement periods, (a) June 8 to 10, 2019; (b) December 17 to 19, 2019.

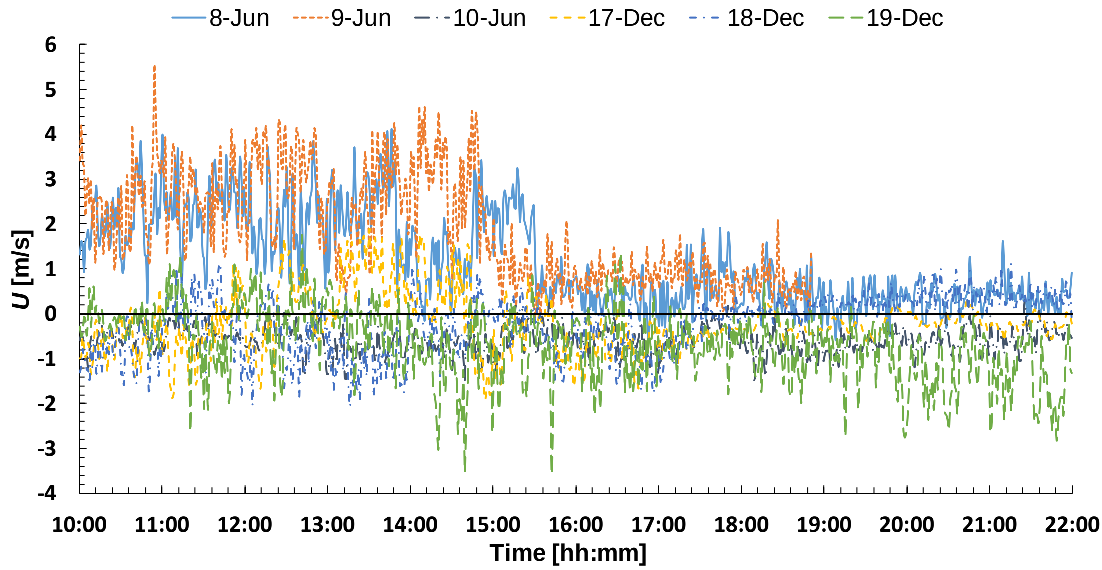

Fig. 7 Temporal-averaged wind velocity component U of the freestream on each day during the summer and winter measurement periods.

Concerning that the ventilation performance and pollutant dispersion were mainly affected by the room locations in the street canyons [35], it is essential to determine the windward and leeward sides of the building model. However, the windward and leeward sides of the building model were dependent on the wind directions. Therefore, when comparing the results between the summer and winter tests, they will be analyzed according to the wind direction of each test. Fig.8 shows the average wind directions and velocities of all tests. The north direction was $0°$ based on the Rainwise weather station, thus, the degree parallel to the street canyons was around $150°$. Fig. 9 shows the categories of the incidence angles of freestream wind relative to the North direction and then the ambient flow in normal, oblique as well as parallel directions are defined. The incoming wind directions of all tests were in a range of $42.3° - 286.3°$, separated by the parallel direction of the street canyons, the tests with the incoming wind between $42.3° - 150°$ had the left side as the windward side, while the tests with the incoming wind between $150° - 286.3°$ had the right side as the windward side.

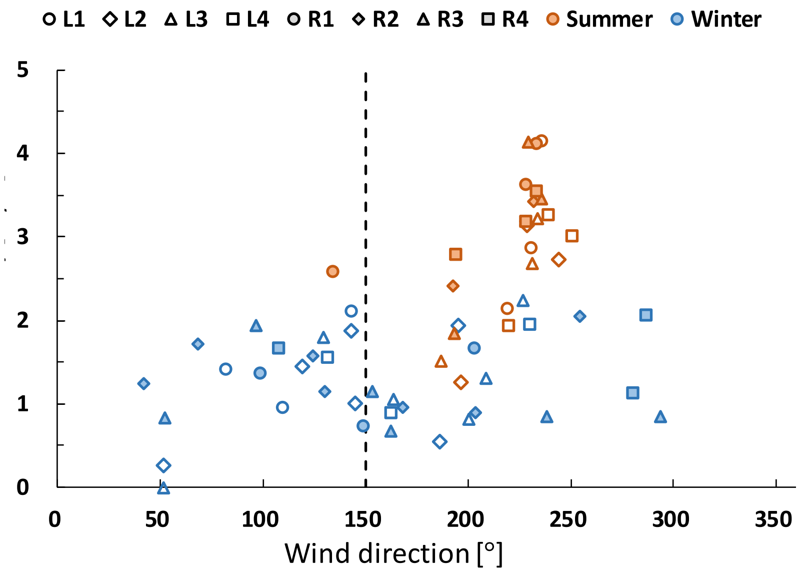

Fig. 8 The average wind directions and velocities of each test during summer and winter periods.

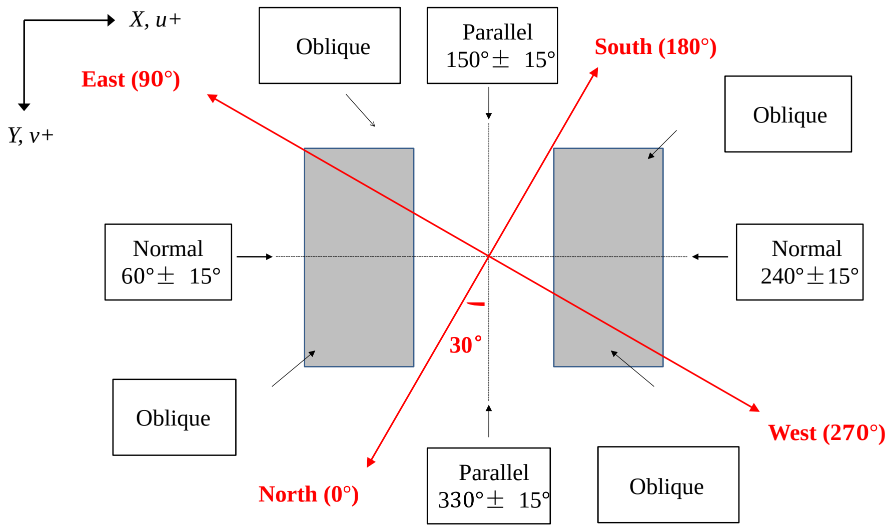

Fig. 9 Categories of the incidence angles of freestream airflows relative to the North directions on X–Y plane.

3.2 Thermal conditions during test periods

Indoor air temperature, outdoor air temperature and surface temperature were monitored during the test periods with thermocouples. Since the air temperature and surface temperature are mainly determined by solar radiation, the room orientation and the street wall orientation are important factors in the temperature distributions in the street canyons. The instant temperature of two measuring days (June 9 and December 18, 2019) are shown in Fig. 10, the data were averaged in 60s. The air temperature and surface temperature were measured by thermocouples at four heights ($z = 0.15m$, $0.45m$, $0.75m$, $1.05m$). Noted that, the surface temperature was measured on the building model, which was made of acrylic and covered with tinfoil. The results will be different from the wall temperature of the concrete models, but they can still represent the thermal conditions in and around the building model.

For the summer tests, the indoor air temperature of rooms at the same height on west side (L1-L4) was generally higher than on the east side (R1-R4). The surface temperature of the summer tests had a similar trend for most of the measuring time, except for a short period (around 15:00-16:00), as shown in Fig. 10(a2). In addition, the indoor air temperature and surface temperature on the west side were obviously increased with heights. In the middle of the street canyon, the differences in the outdoor air temperature at various heights were not significant. While for the winter tests, the indoor air temperature and surface temperature distributions were more complex, they did not show obvious trends with the measuring positions. However, in the middle of the street canyon, the outdoor air temperature was noticeably increased with the measuring heights.

Generally, the thermal conditions among the summer and winter tests were complicated, which cannot estimate the strength of buoyancy effects simply by measurement periods. The results of the thermal condition in this street canyon were dependent on the room locations and measurement time, this will lead to diverse buoyancy effects between indoors and outdoors of different tests.

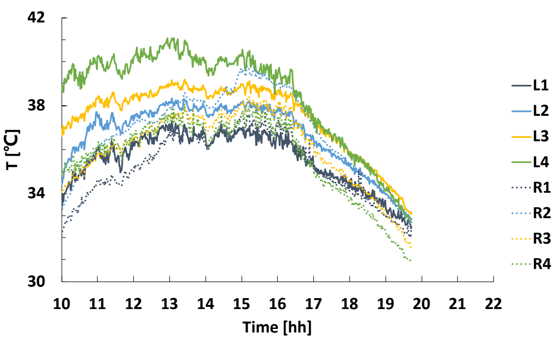

(a1) Indoor air temperature on Jun-9.

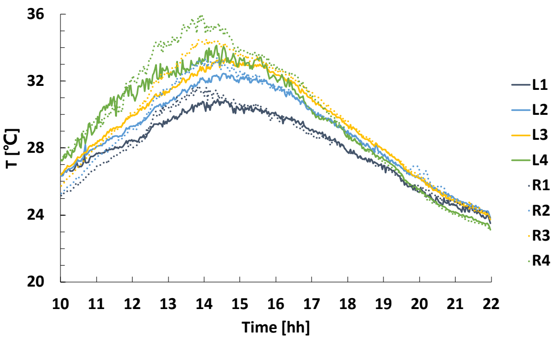

(b1) Indoor air temperature on Dec-18.

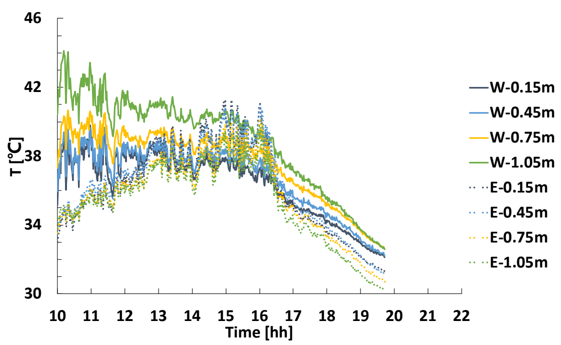

(a2) Surface temperature on Jun-9.

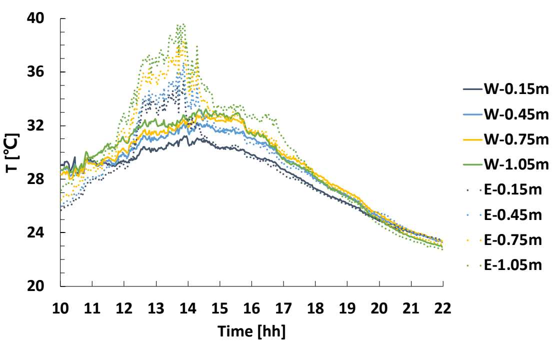

(b2) Surface temperature on Dec-18.

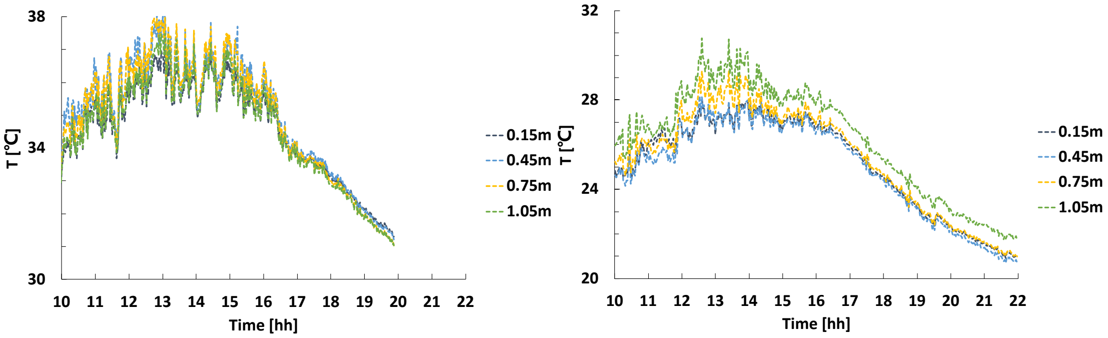

(a3) Outdoor air temperature on Jun-9 Jun. (b3) Outdoor air temperature on Dec-18.

Fig.10 Examples of temperature information during two experiment periods: (a) data from Jun-9., (b) data from Dec-18. (E stands for east wall and W stands for west wall, for example, E-0.15m means east wall temperature at the height of 0.15m)

Fig. 11 shows the indoor air temperature and air temperature differences of each test. The symbols (× and ○) in Fig. 11(a) indicate the average value of the indoor air temperature of each test during the summer and winter periods, respectively. The symbols (△ and ◇) in Fig. 11(b) indicate the indoor and outdoor temperature difference (ΔT) of each test. ΔT is calculated by $\Delta T = T_{in\,z} - T_{out\,z}$, where $T_{in\,z}$ represents the indoor air temperature on each floor, and $T_{out\,z}$ represents the outdoor air temperature at the corresponding height. Caused by the solar heat gain, the average indoor temperature was mostly higher than the outdoor temperature. For the summer measurements, the average indoor air temperatures were found in a range of $31.2 - 40.7$°C. Despite the high indoor temperatures, the temperature differences ΔT mainly varied from $-0.8\,K$ to $3.3\,K$. Only in one test (shown in L4), the temperature difference was up to $5\,K$. Whereas in the winter measurements, the average indoor air temperatures were in a range of $16.9 - 35.0$°C, the temperature differences varied from $1.3\,K$ to $6.4\,K$, as shown in Fig. 11(b). It indicates that the indoor and outdoor air temperature differences of the tests in the winter period at this experiment field were generally larger than in the summer period. It further implies that the buoyancy effect of the winter tests was stronger than summer tests. The high temperature is often associated with the strong buoyancy force, however, in the concrete 2D street canyons, the concrete models and ground absorbed the strong solar radiation and caused the air temperature in the street canyons to heat up drastically [44], which reduced the differences between indoor and outdoor air temperatures. In the winter measurements, the climate temperature and solar radiation were both lower than the summer period, but the effect of heat storage of the building model caused the indoor air temperature to rise up and lead to larger air temperature differences.

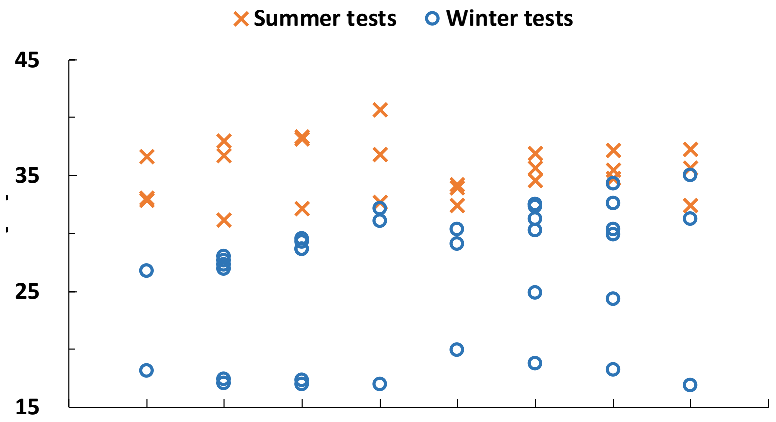

(a)

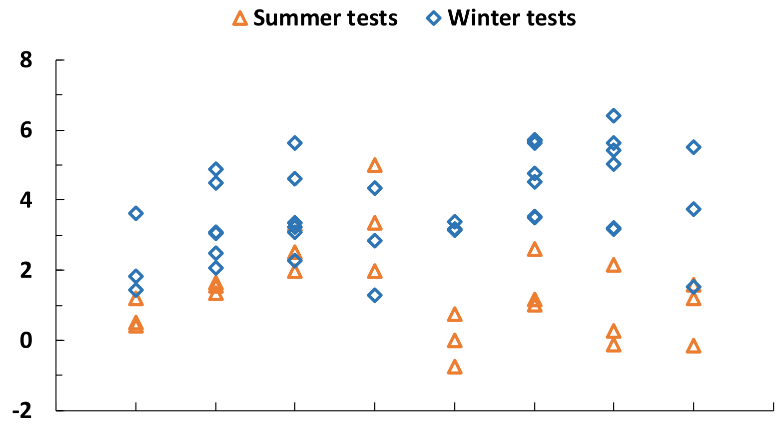

(b)

Fig. 11 The air temperature information of each test during summer and winter measurements, (a) the average indoor air temperature; (b) temperature differences between indoor and outdoor air.

3.3 Ventilation rates of source rooms

3.3.1 Influence of the wind effect

Without considering the influence of the buoyancy effect, the wind effect is the important driving force of the air movement in the urban environment. Fig. 12 shows the ventilation rates calculated from Equation (4) of each test with the changes of wind velocities. The data from the initial $60s$ measurement were excluded. Three observations can be made based on the comparisons of the tests with normal wind direction. First, on the windward side, when the wind velocity was smaller than $3m/s$, the ventilation rate increased with the room floor getting upward basically, as shown in Fig. 12(a). This indicated that the ventilation performance on the windward rooms in the street canyon was positively correlated with the height of the room. This result was consistent with our former work [35]. However, Yang et al. [37] found the results different, they concluded that no obvious regularity can be determined with the windward rooms in street canyons. This paradox may attribute to their adoption of the tracer gas decay method. The tracer gas decay process in their experimental model was very fast and only allowed to measure the ventilation rate in a limited time period, which highly depended on the instant air fluctuations and may not be representative of the average air exchange rate.

Second, when the source was located on the leeward side, the ventilation rates of 2, 3, 4 floors were generally lower than the windward side, while the first floor had a larger ventilation rate than the windward side. Also, the differences in ventilation performance of rooms on of 2, 3, 4 floors were slight, as shown in Fig. 10(b), which indicated that the perpendicular near-wall airflows were nearly uniform and weaker than the windward side.

Third, the ventilation rates of the second and third floors on the windward side were increased with the wind velocity getting larger. The increasing trend was nearly linear when the wind velocity was smaller than $3m/s$, but the trend got slow when the wind velocity was over $3m/s$. Also, considering the ventilation results of both first and fourth floors, when the wind velocity was over $3m/s$, the larger wind velocity may not guarantee larger ventilation rates. It may be because, in the street canyon, a strong incoming wind may create a vertical downwash on the windward side, which can reduce the interaction between the indoor and ambient air. When the incoming wind velocity is higher than a specific value, the ventilation rates no longer increase drastically and may fluctuate within a small range. However, this trend was not shown on the leeward side rooms similarly. The ventilation rates of the leeward tests were more stable and the changes with different wind velocities were not obvious.

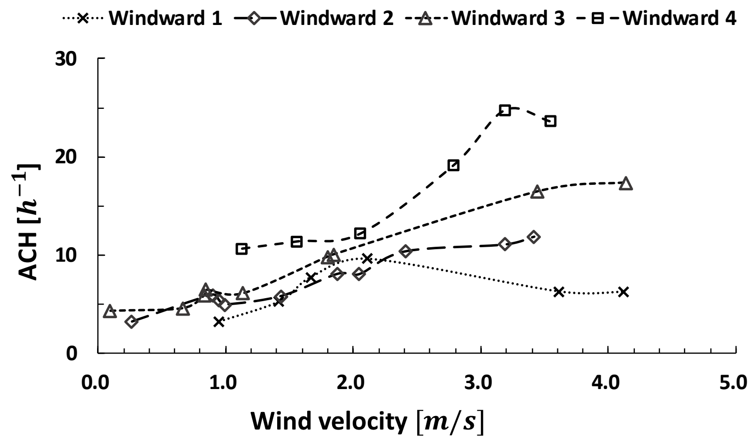

(a)

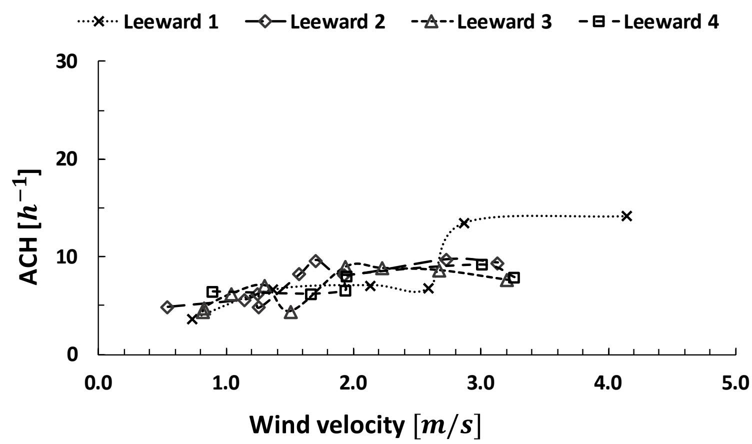

(b)

Fig. 12 Ventilation rates of each test with the wind velocities: (a) windward side rooms; (b) leeward side rooms.

3.3.2 Interactions between buoyancy and wind effects

Wind force and buoyancy forces are two main driving forces in urban ventilations and pollutant dispersion. Concerning the temperature difference between indoors and outdoors in the street canyons, the non-dimensional parameter Archimedes number (Ar) is used. The Archimedes number is a ratio of the buoyancy and inertia forces, which is defined as [45]

$$Ar = \frac{g \cdot \beta \cdot |\Delta T| \cdot H_w}{U^2{}_{ref}} = \frac{g \cdot \beta \cdot H_w |(T_{in\,Z} - T_{out\,Z})|}{U^2{}_{ref}} \tag{6}$$

where g is the gravitational acceleration (m^2/s), $\beta = 1/T_{in\,Z}$ is the thermal expansion coefficient ($1/K$), ΔT is calculated using $\Delta T = T_{in\,Z} - T_{out\,Z}$, $T_{in\,Z}$ represents the indoor air temperature (°C) on each floor, and $T_{out\,Z}$ represents the outdoor air temperature (°C) at the corresponding height, H_w is the window height (m) and U_{ref} is the freestream horizontal velocity (m/s).

The flow rate (m^3/s) caused by the buoyancy effect for the single-sided ventilation can be calculated as [46]

$$Q_B = \frac{1}{3} C_D \cdot A_w \cdot \sqrt{g \cdot \beta \cdot H(T_{in\,Z} - T_{out\,Z})} \tag{7}$$

where C_D is the discharge coefficient usually considered as 0.6, and A_w is the area of the window (m^2).

Without the influence of wind effect, the non-dimensional ventilation rate is induced and defined as

$$Q^* = \frac{Q}{U_{ref} \cdot A_w} \tag{8}$$

where Q is the airflow rate (m^3/s) measured from each test, and U_{ref} is the freestream horizontal velocity (m/s).

Combining Equation (6), (7) and (8), the non-dimensional ventilation rate of the buoyancy effect can be derived as

$$Q_B{}^* = 0.2Ar^{0.5} \tag{9}$$

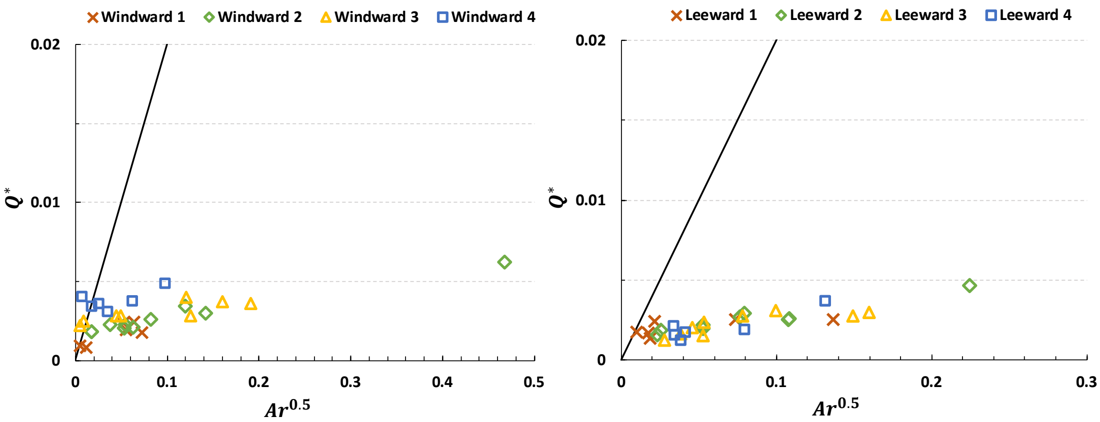

(a) Windward side (b) Leeward side

Fig.13 Relation of the non-dimensional ventilation rate (Q^*) with the square root of the Archimedes number ($Ar^{0.5}$) of each test, (a) tests on the windward side; (b) teats on the leeward side..

Fig.13 can be used to examine the interaction between the buoyancy effect and the wind effect, Equation (9) is drawing as a straight line on this figure. Three areas can be identified from this figure [47]: (1) the area close to the straight line represents the ventilation rate that is mainly driven by the buoyancy effect. (2) the area below the straight line represents the ventilation rate that is smaller than which caused by the buoyancy effect only; the wind effect counteracts the buoyancy effect and reduces the ventilation rate. (3) the area above the straight line represents the ventilation rate that is larger than which caused by the buoyancy effect only; the wind effect strengthens the buoyancy effect and increases the ventilation rate.

Fig. 13 shows the relation of the non-dimensional ventilation rate (Q^*) with the square root of the Archimedes number ($Ar^{0.5}$). When the source was located on the windward side, as shown in Fig. 13(a), most of the Q^* points are below the straight line except for the points with very small $Ar^{0.5}$ ($Ar^{0.5} < 0.05$). This indicates that the interactions between the buoyancy and wind effects were destructive, the combining effect reduced the ventilation rates. Also, when $Ar^{0.5} < 0.2$, the deviations of Q^* were small, which implied the buoyancy effect was not obvious in this street canyon. When the source was located on the leeward side, as shown in Fig. 13(b), similar trends can be found. All the presented Q^* values were below the line $Q_B{}^* = 0.2Ar^{0.5}$.

Several explanations can be made for the results. First, most of the reference wind velocities measured in these experiments were larger than $0.5 m/s$ and the range of the temperature differences were not very large ($1.3K$ to $6.4K$), which caused most $Ar^{0.5}$ values of the test results below 0.2. The limited number of tests during the two experiment periods did not catch enough cases with the low wind and high-temperature differences. Second, the discharge coefficients C_D in Equation (7) adopted 0.6, which was according to the empirical value measured in full-scale measurements [48-50]. However, some research [51, 52] reported that the discharge coefficients have smaller values in scaled models, varying from 0.13 to 0.207. This may also affect the results of the interactions between the buoyancy and wind effects in the scaled street canyons. The detailed ventilation performance of scaled models needs further investigation.

Since the buoyancy force is mainly going upwards, the combined wind and buoyancy effect may have two conditions in the street canyons: first, on the windward side, the airflow mainly flushes downward [35], which is in the opposite direction with the buoyancy force, the buoyancy force will be countered by the wind force; second, on the leeward side, the airflow mainly goes upward [35], which is in the same direction with the buoyancy force [53], the upward force will be strengthened. The proportion of the buoyancy force and the wind force was delicate in the outdoor environment, with the opening height of the scaled building model as $0.1m$, the stack effect through the openings may not be strong enough to cause variation of the tracer gas concentrations. As a result, the characteristics of the ventilation performance by the buoyancy effect were not apparently shown with the experiment data.

3.4 Interunit dispersion characteristics and implications

The interunit dispersion characteristics of one day (June 9, 2019) during the summer measurements have been analyzed in our previous, and it implied the correlation between the tracer gas dispersion and the source locations [35]. In the present study, the characteristics of the interunit dispersion with the wind effect in street canyons were further investigated.

Fig. 14 shows the non-dimensional CO_2 concentration results of each room with the increasing wind velocities. $\overline{U}$ represents the average incoming wind velocity in the perpendicular direction to the street canyons (60° and 240°), as shown in Fig. 9. As per Equation (5), the term K_c represents the average non-dimensional CO_2 concentration of each room during different tests. It indicates the level of the tracer gas transmissions from the source room to other rooms. The results show that K_c of each room varied drastically with the source location, room location and wind velocities. Several observations can be made from the comparisons of the results.

First, the wind was an important driving force for the tracer gas transmission, however, larger wind velocities did not simply increase or decrease the levels of CO_2 concentration in the reentered rooms. For most of the tests, when the wind velocity was over a certain value, the CO_2 concentration of the reentered rooms decreased or maintained the same level. The large turbulent momentum accelerated the tracer gas dispersion in the source rooms and blocked them from further reentering other rooms. However, this phenomenon was not found in the tests with source room of Leeward 4 (L4-a), as shown in Fig. 14(h), K_c results of $\overline{U}$ equal to $3.3m/s$ stated an obvious upward trend. Compared to the tests with $\overline{U}$ equal to $3.0m/s$ (L4-c), the conditions of test L4-a contained a higher temperature difference ($5.0K$, $3.3K$ in test L4-c), also, the ventilation rate of the source room Leeward 4 was lower ($7.9h^{-1}$, $9.2h^{-1}$ in test L4-c). This may be because that the higher buoyancy force will restrain the tracer gas dispersion of the source room in the scaled outdoor models, so that the pollutants may have a higher possibility to reenter other rooms.

Second, when the wind velocity was lower than a certain value, the tracer gas transmission was more complicated. For most of the tests, larger $\overline{U}$ will increase the CO_2 concentration of the reentered rooms with the wind velocity under $1.0m/s$. The results of the source locations in room Leeward 1 and 2 were exceptions, as shown in Fig. 14(b) and (d). In these tests, the lower wind velocities revealed higher reentered tracer gas concentrations.

Then, the results of CO_2 concentration in the reentered rooms varied significantly in different tests. Except for the wind velocity and temperature differences, the source room location was another important parameter that affected the level of CO_2 concentrations. With the increasing wind velocities, the different source locations lead to variable characteristics of the CO_2 concentration in the reentered rooms. Our previous study [35] concluded that the highest tracer gas concentration occurred generally in the room nearest to the source room along the transportation route. In the present study, the results were mostly consistent with the former conclusion. But the tests of source location at room Leeward 3, as shown in Fig. 14(f), and the tests with $\overline{U}$ under $1.0m/s$ of source locations at room Windward 2 and 3, as shown in Fig. 14(c) and (e), show different results. When the source room was located in the middle height of the street canyon, the pollutant dispersion routes will mainly rely on the vortex direction. In the conditions of $\overline{U}$ under $1.0m/s$, it was highly possible that the stable vortex was not formed inside the street canyon, which caused the irregular tracer gas transportation routes in the tests of source location at room Windward 2 and 3.

Finally, the results of most tests demonstrated relatively clear and similar trends of each reentered room, except for the source location of room Windward 2 and Leeward 3. Especially in the tests of Leeward 3, K_c results of the other three reentered rooms fluctuated drastically. Several causes may account for this condition. In the real atmospheric environment, the incoming wind directions highly fluctuated, the significant changes in wind direction may attribute to the tracer gas dispersing in multiple directions and spread randomly. Also, as stated formerly, the small wind velocity did not form a stable vortex in the street canyon, which caused the disordered transmission characteristics.

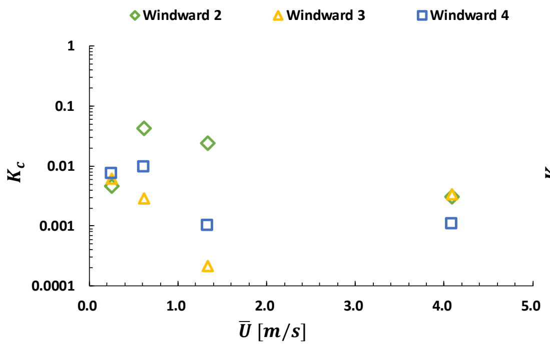

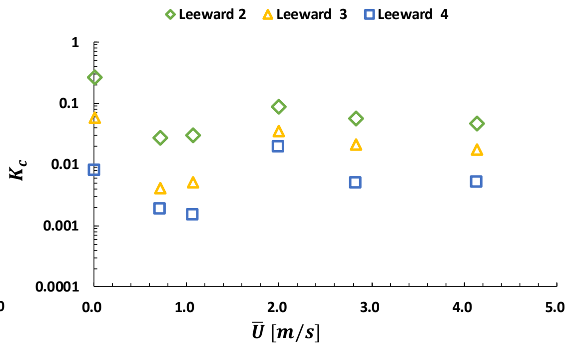

(a) Source room: Windward 1

(b) Source room: Leeward 1

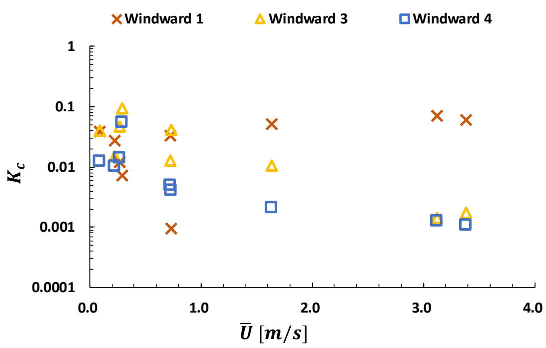

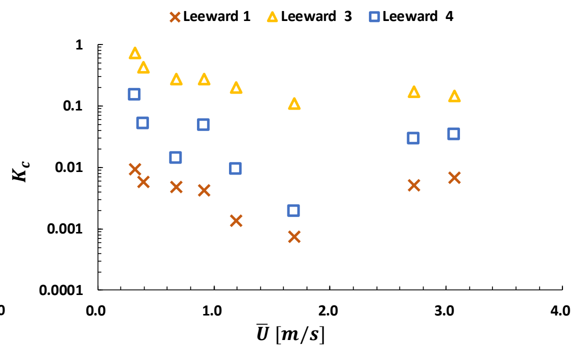

(c) Source room: Windward 2

(d) Source room: Leeward 2

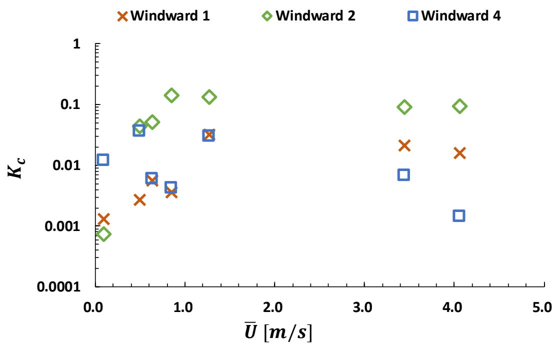

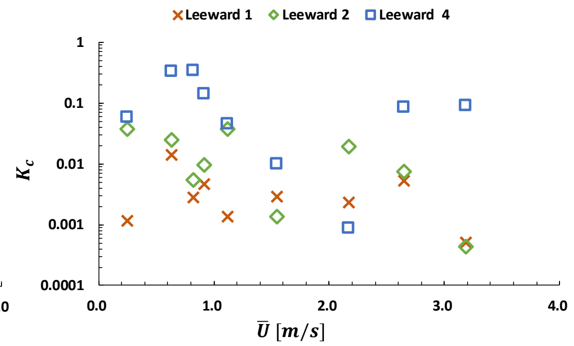

(e) Source room: Windward 3

(f) Source room: Leeward 3

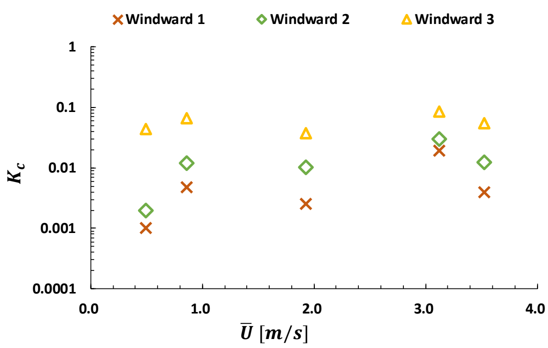

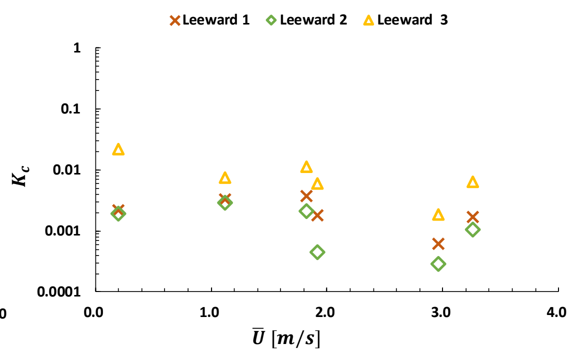

(g) Source room: Windward 4 (h) Source room: Leeward 4

Fig. 14 Non-dimensional CO_2 concentration (K_c) results of each reentered room with increase in $\overline{U}$ with different source locations.

4. Limitations

In this study, we experimentally investigate the ventilation rate and pollutant dispersion in street canyons ($H/W = 1$) with wind and buoyancy effects. The experiment field was located in a suburban area of Guangzhou, a typical subtropical region. In such experiment field, the measurements in both summer and winter periods did not acquire a number of tests with very large indoor and outdoor temperature differences. With the limited number of tests, the influence of the combined wind and buoyancy effects on the pollutant dispersion was not obviously shown by the experiment data, which needs further investigations.

For the scaled models used in the experiment, most of the tests had higher indoor air temperature than outdoors, which can only represent one condition of the buoyancy force. The reverse condition (higher outdoor air temperature than indoors) was not included in the experiments.

In addition, under the real atmospheric boundary conditions, the wind velocities and directions fluctuated constantly. However, the pollutant transmission between rooms may partly depend on the instant wind and buoyancy conditions. Therefore, the analysis with averaged wind velocities of each test cannot reveal the transient pollutant transmission between rooms. The short-term process of pollutant dispersion in the street canyons will be studied in the future with CFD simulations.

5. Conclusions

This study conducted scaled outdoor experiments in summer and winter periods to explore the single-sided ventilation performance and the pollutant transmission in 2D street canyons ($H/W = 1$) with the tracer gas method. Two periods of the measurements were performed to investigate the influence of the wind effect and the combined wind and buoyancy effects on the interunit dispersion. The ventilation rates were acquired by the constant releasing of the tracer gas, and the interunit dispersion was revealed by the tracer gas concentrations. The non-dimensional buoyancy parameter, Archimedes number Ar, was induced to examine the interactions of the buoyancy force and the wind force caused by the indoor and outdoor air temperature differences.

The conclusions can be drawn as follows:

(1) The wind and thermal conditions of the summer and winter experiments were different. The wind velocities of the summer period were generally larger than the winter period. The indoor air temperatures of the summer test were also larger than winter tests, but the indoor and outdoor air temperature differences

of the winter periods were higher than summer, which resulted in stronger buoyancy forces in the winter measurements.

(2) The ventilation performance of the windward and leeward rooms showed different trends with the wind velocity. When the incoming wind velocity was smaller than a certain value, the ventilation rates of the windward rooms were increased linearly with the wind velocity getting larger. But when the wind velocity exceeded this value, the ventilation rates no longer increase drastically. However, the ventilation performance of the leeward tests was more stable and the changes with different wind velocities were not obvious.

(3) With the square root of the Archimedes number ($Ar^{0.5}$), the non-dimensional ventilation rates (Q^*) of both windward and leeward rooms were generally smaller than the buoyancy effect only. It indicates that interactions between the buoyancy and wind effects were destructive, the combining effect reduced the ventilation rates. In addition, the increase of Q^* was small when $Ar^{0.5} < 0.2$, which implied the buoyancy effect was not obvious during the two measurement periods.

(4) The interunit dispersion characteristics with the wind effect were highly dependent on the source locations, room location and wind velocities in the street canyons. Different source locations lead to variable characteristics of the CO_2 concentration in the reentered rooms. The pollutant dispersion routes mainly rely on the vortex formation and vortex direction in the street canyon. In addition, larger wind velocities did not simply increase or decrease the tracer gas concentration in the reentered rooms.

Acknowledgement

The experiment described in this paper was conducted at Sun Yat-sen University. It is declared that all authors do not have a conflict of interest. This study was financially supported by Shanghai Sailing Program (NO. 21YF1430700), National Natural Science Foundation of China (No. 41875015, 41805102), Special fund for science and technology innovation strategy of Guangdong Province (International cooperation) (China, No 2019A050510021) and the Key projects of Guangdong Natural Science Foundation (China, No. 2018B030311068).

References:

1. A.M. Rahmani, and S.Y.H. Mirmahaleh, Coronavirus disease (COVID-19) prevention and treatment methods and effective parameters: A systematic literature review. Sustainable cities and society, 2020. p.102568.
2. Y.X. Li, R.Y. Zhang, J.Y. Zhao and M.J. Molina, Understanding transmission and intervention for the COVID-19 pandemic in the United States. Science of The Total Environment, 2020. 748: p. 141560.

3. C. Sun and Z. Zhai, The efficacy of social distance and ventilation effectiveness in preventing COVID-19 transmission. Sustainable cities and society, 2020. 62, p.102390.
4. Y. Liu, Z. Ning, Y. Chen, M. Guo, Y.L. Liu, N.K. Gali, L. Sun, Y.S. Duan, J. Cai, D. Westerdahl, X.J. Liu, K. Xu, K.F. Ho, H.D. Kan, Q.Y. Fu and K. Lan, Aerodynamic analysis of SARS-CoV-2 in two Wuhan hospitals. Nature, 2020. 582(7813): p. 557-560.
5. L. Morawska and J. Cao, Airborne transmission of SARS-CoV-2: The world should face the reality. Environment international, 2020. 139, p.105730.
6. K.A. Prather, C.C. Wang and R.T. Schooley, Reducing transmission of SARS-CoV-2. Science, 2020. 368(6498), pp.1422-1424.
7. J.W. Tang, Y. Li, I. Eames, P.K.S. Chan and G.L. Ridgway, Factors involved in the aerosol transmission of infection and control of ventilation in healthcare premises. Journal of Hospital Infection, 2006. 64(2): p. 100-114.
8. Y. Li, M. Leung, J.W. Tang, X. Yang, C.Y.H. Chao, J.Z. Lin, J.W. Lu, P.V. Nielsen, J. Niu, H. Qian, A.C. Sleigh, H.-J.J. Su, J. Sundell, T.W. Wong and P.L. Yuen, Role of ventilation in airborne transmission of infectious agents in the built environment - a multidisciplinary systematic review. Indoor air, 2007. 17(1): p. 2-18.
9. Y. Li, D.Y. Leung, W. Tam, A.T. Chan, T.W. Wong, T. Ho, I.T. Yu and J.H. Lee, Evidence of airborne transmission of the severe acute respiratory syndrome virus. New England Journal of Medicine, 2004. 350(17): p. 1731-1739.
10. J. Niu and T.C.W. Tung, On-site quantification of re-entry ratio of ventilation exhausts in multi-family residential buildings and implications. Indoor Air, 2008. 18(1): p. 12-26.
11. H.L. Gough, Z. Luo, C.H. Halios, M.F. King, C.J. Noakes, C.S.B. Grimmond, J.F. Barlow, R. Hoxey and A.D. Quinn, Field measurement of natural ventilation rate in an idealised full-scale building located in a staggered urban array: Comparison between tracer gas and pressure-based methods. Building and Environment, 2018. 137, pp.246-256.
12. Y. Wu, T.C.W. Tung and J.L. Niu, On-site measurement of tracer gas transmission between horizontal adjacent flats in residential building and cross-infection risk assessment. Building and Environment, 2016. 99: p. 13-21.
13. Y. Wu, T.C.W. Tung and J.L. Niu, Experimental analysis of driving forces and impact factors of horizontal inter-unit airborne dispersion in a residential building. Building and Environment, 2019. 151: p. 88-96.
14. J.H. Wang, J.L. Niu, X.P. Liu and C.W.F. Yu, Assessment of pollutant dispersion in the re-entrance space of a high-rise residential building, using wind tunnel simulations. Indoor and Built Environment, 2010. 19(6): p. 638-647.
15. D. Mu, C. Shu, N.P. Gao and T. Zhu, Wind tunnel tests of inter-flat pollutant transmission characteristics in a rectangular multi-storey residential building, part B: Effect of source location. Building and Environment, 2017. 114: p. 281-292.
16. X.P. Liu, J.L. Niu, K.C.S. Kwork, J.H. Wang and B.Z. Li, Investigation of indoor air pollutant dispersion and cross-contamination around a typical high-rise

residential building: Wind tunnel tests. Building and environment, 2010. 45(8): p. 1769-1778.
17. L. Li and C.M. Mak, The assessment of the performance of a windcatcher system using computational fluid dynamics. Building and environment, 2007. 42(3): p. 1135-1141.
18. X.P. Liu, J.L. Niu, M. Perino and P. Heiselberg, Numerical simulation of inter-flat air cross-contamination under the condition of single-sided natural ventilation. Journal of Building Performance Simulation, 2008. 1(2): p. 133-147.
19. N.P. Gao, J.L. Niu, M. Perino and P. Heiselberg, The airborne transmission of infection between flats in high-rise residential buildings: Tracer gas simulation. Building and Environment, 2008. 43(11): p. 1805-1817.
20. N.P. Gao, J.L. Niu, M. Perino and P. Heiselberg, The airborne transmission of infection between flats in high-rise residential buildings: Particle simulation. Building and Environment, 2009. 44(2): p. 402-410.
21. X. Yang, K. Zhong, Y. Kang and T. Tao, Numerical investigation on the airflow characteristics and thermal comfort in buoyancy-driven natural ventilation rooms. Energy and Buildings, 2015. 109, pp.255-266.
22. Z.T. Ai and C.M. Mak, A study of interunit dispersion around multistory buildings with single-sided ventilation under different wind directions. Atmospheric Environment, 2014. 88: p. 1-13.
23. Z.T. Ai and C.M. Mak, Large eddy simulation of wind-induced interunit dispersion around multistory buildings. Indoor air, 2016. 26(2): p. 259-273.
24. Z.T. Ai, C.M. Mak and J.L. Niu, Numerical investigation of wind-induced airflow and interunit dispersion characteristics in multistory residential buildings. Indoor air, 2013. 23(5): p. 417-429.
25. J. Wang, S. Wang, T. Zhang and F. Battaglia, Assessment of single-sided natural ventilation driven by buoyancy forces through variable window configurations. Energy and buildings, 2017. 139, pp.762-779.
26. J. Wang, S. Wang, T. Zhang and F. Battaglia, Gaseous pollutant transmission through windows between vertical floors in a multistory building with natural ventilation. Energy and buildings, 2017. 153, pp.325-340.
27. D.J. Cui, C.M. Mak, K.C.S. Kwok and Z.T. Ai, CFD simulation of the effect of an upstream building on the inter-unit dispersion in a multi-story building in two wind directions. Journal of Wind Engineering and Industrial Aerodynamics, 2016. 150: p. 31-41.
28. Y.W. Dai, C.M. Mak and Z.T. Ai, Computational fluid dynamics simulation of wind-driven inter-unit dispersion around multi-storey buildings: Upstream building effect. Indoor and Built Environment, 2019. 28(2): p. 217-234.
29. D. Mu, N.P. Gao and T. Zhu, CFD investigation on the effects of wind and thermal wall-flow on pollutant transmission in a high-rise building. Building and Environment, 2018. 137: p. 185-197.

30. Y.W. Dai, C.M. Mak and Z.T. Ai, Flow and dispersion in coupled outdoor and indoor environments: Issue of Reynolds number independence. Building and Environment, 2019. 150: p. 119-134.
31. A. Dallman, S. Magnusson, R. Britter, L. Norford, D. Entekhabi and H.J.S. Fernando, Conditions for thermal circulation in urban street canyons. Building and Environment, 2014. 80: p. 184-191.
32. E. Yee and C.A. Biltoft, Concentration fluctuation measurements in a plume dispersing through a regular array of obstacles. Boundary-Layer Meteorology, 2004. 111(3): p. 363-415.
33. G.W. Chen, X. Yang, H.Y. Yang, J. Hang, Y.Y. Lin, X.M. Wang, Q. Wang and Y.L. Liu, The influence of aspect ratios and solar heating on flow and ventilation in 2D street canyons by scaled outdoor experiments. Building and Environment, 2020. 185: p. 107159.
34. G.W. Chen, D.Y. Wang, Q. Wang, Y.G. Li, X.M. Wang, J. Hang, P. Gao, C.Y. Ou and K. Wang, Scaled outdoor experimental studies of urban thermal environment in street canyon models with various aspect ratios and thermal storage. Science of The Total Environment, 2020. 726: p. 138147.
35. Y.W. Dai, C.M. Mak, Y. Zhang, D.J. Cui and J. Hang, Investigation of interunit dispersion in 2D street canyons: A scaled outdoor experiment. Building and Environment, 2020. 171: p. 106673.
36. Y. Zhang, Z. Gu and C.W. Yu, Review on numerical simulation of airflow and pollutant dispersion in urban street canyons under natural background wind condition. Aerosol and Air Quality Research, 2018. 18(3), pp.780-789.
37. X. Yang, J. Hang, C. Ou and P. Gao, Measurement of air change rate in single-sided building by Scale-model outdoor experiments, in The 16th Conference of the International Society of Indoor Air Quality & Climate (Indoor Air 2020) COEX. 2020: Seoul, Korea.
38. X. Liu, X. Lv, Z. Peng and C. Shi, Experimental study of airflow and pollutant dispersion in cross-ventilated multi-room buildings: Effects of source location and ventilation path. Sustainable Cities and Society, 2020. 52: p. 101822.
39. W. Köppen and R. Geiger, Handbuch der klimatologie. Vol. 1. 1930: Gebrüder Borntraeger Berlin.
40. P.M. Congedo, C. Baglivo, A.K. Seyhan and R. Marchetti, Worldwide dynamic predictive analysis of building performance under long-term climate change conditions. Journal of Building Engineering, 2021. 42, p.103057.
41. D. Chen and H.W. Chen, Using the Köppen classification to quantify climate variation and change: An example for 1901–2010. Environmental Development, 2013. 6, pp.69-79.
42. X.X. Li, Leung, Y.C. Dennis, C.H. Liu and K.M. Lam, Physical modeling of flow field inside urban street canyons. Journal of Applied Meteorology and Climatology, 2008. 47(7): p. 2058-2067.

43. W.H. Snyder, Guideline for fluid modeling of atmospheric diffusion. Vol. 81. 1981: Environmental Sciences Research Laboratory, Office of Research and Development, US Environmental Protection Agency.
44. S. Magnusson, A. Dallman, D. Entekhabi, R. Britter, H.J.S. Fernando and L. Norford, On thermally forced flows in urban street canyons. Environmental Fluid Mechanics, 2014. 14(6): p. 1427-1441.
45. P. Warren, Single-sided ventilation through open window. ASHRAE SP49, 1985.
46. T.S. Larsen and P. Heiselberg, Single-sided natural ventilation driven by wind pressure and temperature difference. Energy and Buildings, 2008. 40(6): p. 1031-1040.
47. M. Caciolo, S. Cui, P. Stabat and D. Marchio, Development of a new correlation for single-sided natural ventilation adapted to leeward conditions. Energy and buildings, 2013. 60, pp.372-382.
48. P. Heiselberg, K. Svidt and P.V. Nielsen, Characteristics of airflow from open windows. Building and Environment, 2001. 36(7): p. 859-869.
49. F. Flourentzou, J. Van der Maas and C.A. Roulet, Natural ventilation for passive cooling: measurement of discharge coefficients. Energy and buildings, 1998. 27(3): p. 283-292.
50. B.M. Jones, M.J. Cook, S.D. Fitzgerald and C.R. Iddon, A review of ventilation opening area terminology. Energy and Buildings, 2016. 118: p. 249-258.
51. G. Lane-Serff, Heat flow and air movement in buildings, 1989. University of Cambridge.
52. D. Kiel and D. Wilson, Combining door swing pumping with density driven flow. ASHRAE Transactions, 1989. 95(2): p. 590-599.
53. J. Park, J. Choi and G.H. Rhee, Effect of wind and buoyancy interaction on single-sided ventilation in a building. Journal of Wind Engineering and Industrial Aerodynamics, 2017. 171: p. 380-389.